Crystal Structure of Leucotoxin S Component

Valérie Guillet, Pierre Roblin, Sandra Werner, Manuela Coraiola, Gianfranco Menestrina, Henri Monteil, Gilles Prévost, Lionel Mourey

THE JOURNAL OF BIOLOGICAL CHEMISTRY
Vol. 279, No. 39, Issue of September 24, pp. 41028–41037, 2004

Printed in U.S.A.

Crystal Structure of Leucotoxin S Component

NEW INSIGHT INTO THE STAPHYLOCOCCAL β-BARREL PORE-FORMING TOXINS*

Received for publication, June 21, 2004, and in revised form, July 14, 2004
Published, JBC Papers in Press, July 18, 2004, DOI 10.1074/jbc.M406904200

Valérie Guillet‡, Pierre Roblin‡, Sandra Werner§, Manuela Coraiola¶, Gianfranco Menestrina¶, Henri Monteil§, Gilles Prévost§‖, and Lionel Mourey‡**

From the ‡Groupe de Biophysique Structurale, Département Mécanismes Moléculaires des Infections Mycobactériennes, CNRS-IPBS, 205 route de Narbonne, 31077 Toulouse Cedex, France, the §Laboratoire de Physiopathologie et d'Antibiologie des Infections Bactériennes Emergentes et Nosocomiales-EA 3432, Institut de Bactériologie de la Faculté de Médecine, Hôpitaux Universitaires de Strasbourg, 3 rue Koeberlé, 67000 Strasbourg, France, and the ¶CNR-ITC Istituto di Biofisica Sezione di Trento, Via Sommarive 18 I-38050 Povo, Italy

Staphylococcal leucocidins and γ-hemolysins (leucotoxins) are bi-component toxins that form lytic transmembrane pores. Their cytotoxic activities require the synergistic association of a class S component and a class F component, produced as water-soluble monomers that form hetero-oligomeric membrane-associated complexes. Strains that produce the Panton-Valentine leucocidin are clinically associated with cutaneous lesions and community-acquired pneumonia. In a previous study, we determined the crystal structure of the F monomer from the Panton-Valentine leucocidin. To derive information on the second component of the leucotoxins, the x-ray structure of the S protein from the Panton-Valentine leucocidin was solved to 2.0 Å resolution using a tetragonal crystal form that contains eight molecules in the asymmetric unit. The structure demonstrates the different conformation of the domain involved in membrane contacts and illustrates sequence and tertiary structure variabilities of the pore-forming leucotoxins. Mutagenesis studies at a key surface residue (Thr-28) further support the important role played by these microheterogeneities for the assembly of the bipartite leucotoxins.

Among the bacterial β-barrel pore-forming toxins, the subfamily of staphylococcal bicomponent leucotoxins (leucocidins, Luk, and γ-hemolysins, Hlg) include seven class S proteins (LukS-PV, LukS-R, LukE, LukM, HlgA, HlgC, and LukS-I: ≈32 kDa) and six class F proteins (LukF-PV, LukF-R, LukD, LukF'-PV, HlgB, and LukF-I: ≈34 kDa) that are able to synergistically permeabilize human polymorphonuclear cells, monocytes, and macrophages (1). To achieve pore formation, the secreted class S proteins primarily bind to specific membrane receptors whose abundance varies according to the protein kinase C pathway (2–4). This binding followed by that of class F proteins ultimately leads to the formation of bipartite pores that are permeable to monovalent cations. However, before these pores are functional and ensure cell lysis, cell Ca^{2+} channels are activated (5), probably by a signal transduction pathway that allows the secretion of inflammatory compounds (6–9). Genes encoding γ-hemolysins are present in almost all clinical strains, whereas the Panton-Valentine leucocidin, composed of LukS-PV and LukF-PV, is secreted by strains isolated from humans with abscesses, furuncles, and community-acquired pneumonia. Other members, such as LukE-LukD, have been found associated with staphylococcal bullous impetigo of young infants and post-antibiotic diarrhea (1).

Bicomponent leucotoxins are related in sequence, structure, and function to staphylococcal α-hemolysin (33 kDa), the β-barrel pore-former prototype, and similar proteins have also been found in *Clostridium perfringens* and *Bacillus cereus* (10, 11). The crystal structure of the detergent-solubilized α-hemolysin homo-heptamer has been determined at 1.9 Å resolution and revealed details of the assembled toxin (12). The α-hemolysin mushroom-shaped complex is divided in three domains: the cap, the rim, and the stem. The cap consists of the β-sandwich and amino latch from each protomer. It is extended underneath by the rim domains, each consisting of an open face sandwich, that form the base for a direct interaction with lipid bilayers. Each protomer also participates in the stem, the transmembrane β-barrel pore, by a central sequence folded as a β-hairpin. The x-ray structures of the secreted water-soluble monomeric form of two class F proteins, HlgB from γ-hemolysin (13) and LukF-PV from the Panton-Valentine leucocidin (14), were also determined. They revealed a similar overall fold as the α-hemolysin protomer, except that the stem region adopts a more compact conformation, forming three antiparallel β-strands stacked against the β-sandwich domain. Other structural deviations are confined to some connecting loops, to the N and C termini and to the respective orientation of the rim and β-sandwich domains. No high resolution structural information is available for an assembled leucotoxin oligomer whose molecular architecture remains to be precisely elucidated because it was shown that F and S components of γ-hemolysin may form a heterohexamer (15–17), a heteroheptamer (18), or a heterooctamer (17, 19).

Despite the fact that sequence identity between leucotoxins

* This work was supported by Grant EA-3432 from the Direction de la Recherche et des Etudes Doctorales of the UPRES EA-3432 at the Institut de Bactériologie de la Faculté de Médecine de Strasbourg (to G. P.) and funds from the Consiglio Nazionale delle Ricerche and Provincia Autonoma di Trento Fondo Progetti Project Stawars (to G. M. and G. P.). The costs of publication of this article were defrayed in part by the payment of page charges. This article must therefore be hereby marked "*advertisement*" in accordance with 18 U.S.C. Section 1734 solely to indicate this fact.

The atomic coordinates and structure factors (code 1t5r) have been deposited in the Protein Data Bank, Research Collaboratory for Structural Bioinformatics, Rutgers University, New Brunswick, NJ (http://www.rcsb.org/).

This paper is dedicated to the memory of Dr. Gianfranco Menestrina who died accidentally on July 8, 2004 concurrently with the acceptation of this article. He was a true friend and a brilliant and fair mind who inspired respect from the scientific community. We are deeply affected by this fatality.

‖ To whom correspondence may be addressed. Tel.: 33-390-243-757; Fax: 33-388-251-113; E-mail: gilles.prevost@medecine.u-strasbg.fr.

** To whom correspondence may be addressed. Tel.: 33-561-175-436; Fax: 33-561-175-994; E-mail: lionel.mourey@ipbs.fr.

TABLE I
Molecular replacement results

The Eulerian angles (α, β, and γ) and translation components (Tx, Ty, and Tz) of the different solutions are indicated by order of appearance with the corresponding correlation coefficient *C* and *R* factor values, as given by the program MOLREP (24).

Solution	α	β	γ	Tx	Ty	Tz	*R* factor	*C*
1	9.39	166.16	−30.11	0.202	0.049	0.000	0.653	0.151
2	9.39	166.16	−30.11	0.202	0.048	0.507	0.622	0.287
3	0.00	180.00	−1.37	0.802	0.480	0.345	0.600	0.323
4	0.00	180.00	−1.37	0.802	0.481	0.838	0.604	0.355
5	80.65	13.78	149.95	0.545	0.703	0.397	0.598	0.359
6	80.65	13.78	149.95	0.547	0.704	0.903	0.599	0.372
7	0.00	0.00	88.68	0.021	0.699	0.058	0.599	0.382
8	0.00	0.00	88.68	0.019	0.699	0.565	0.591	0.387

F and S components or between F (or S) components and α-hemolysin does not exceed 30%, the available structural data strongly suggest that all these pore-forming proteins, which share the transition from a hydrosoluble state to a membrane-stabilized structure, have evolved from a common ancestor. Based on such evolutionary considerations the different subunit-subunit interfaces found in leucotoxins may be related to the single interface of α-hemolysin (19) and could involve similar geometrical and structural features. Then complementary mutations must have occurred to explain that (i) class S proteins bear specific structural features compatible with membrane ligand binding, (ii) class F proteins combine to previously bound class S proteins to form a functional pore, and (iii) leucotoxin hetero-oligomers may display a wide variety of combinations and permutations (20, 21). The basis of microevolution was also demonstrated by the reversion of the cationic selectivity of γ-hemolysin to an anionic one comparable with that of α-hemolysin (22).

Here we report the three-dimensional structure determination and analysis of the S component of the Panton-Valentine leucocidin (LukS-PV, 284 residues, 32.3 kDa) from a tetragonal crystal form that diffracts x-rays to 2.0 Å (23). The determination of this first three-dimensional structure of a S protein confirms that it resembles that of the F proteins and brings further important details about the subtle variability that can be accommodated within the fold of the pore-forming leucotoxins superfamily. The rim domain, which has been previously suggested to play an important role in membrane binding, constitutes the most structurally heterogeneous part of the F and S structures. In addition, mutagenesis studies performed at Thr-28, a key interface residue, illustrate the impact of microheterogeneity on the structure-function relationships of the β-barrel pore-forming toxins.

EXPERIMENTAL PROCEDURES

Crystallization, Data Collection, and Phasing—A detailed description of the protocols used for purification and crystallization of wild type and recombinant LukS-PV proteins has been published elsewhere (23). Briefly, crystallization was achieved by the hanging drop vapor diffusion method at 285 K with Jeffamine M-600 as the precipitant. Tetragonal crystals of wild type protein were obtained by cross-seeding monoclinic microcrystals of the recombinant protein in a drop prepared by mixing equal volumes of the protein at a concentration of 20–25 mg/ml in 50 mM MES-NaOH,[1] 50 mM NaCl, pH 6.0, and of the reservoir containing 30% (v/v) Jeffamine M-600, 0.1 M Tris-HCl at pH 8.0–8.9. These crystals belong to space group $P4_3$ with cell parameters $a = b = 94.8$ Å, $c = 306.1$ Å and previous calculations based on Matthews coefficient indicated that the asymmetric unit may contain up to 10 molecules. A 2.0-Å resolution native data set was collected from a single crystal at beamline ID14–1 of the European Synchrotron Radiation Facility (Grenoble, France). Molecular replacement was performed in all possible primitive tetragonal space groups using the program MOLREP (24) as implemented in the CCP4 suite of programs (25) and the structure of the Panton-Valentine leucocidin F component (14) (Protein Data Bank entry code 1PVL). The search model was truncated as a polyalanine, except for strictly conserved residues among S and F proteins and loops of the *rim* domain that obviously differ were removed. One solution corresponding to eight molecules in the asymmetric unit was apparent with correlation coefficient (*C*) and crystallographic *R* factor of 0.387 and 0.591, respectively, in the 35.5–3.0 Å resolution range. The final *C* and *R* factor with other space groups than $P4_3$ were not better than 0.253 and 0.617, respectively. The eight molecules in the asymmetric unit can be grouped by pairs (Table I). Within a pair, the two molecules are in the same orientation and related by the translation vector (0, 0, and 0.5). These results were in agreement with the Patterson map computed from the native data set, which displayed the second strongest peak (8% of the origin peak) at (0.0, 0.0365, and 0.5). Crystal packing showed no bad contact between symmetry-related molecules.

TABLE II
Refinement statistics

Resolution (Å)	35.5–2.0
No of molecules in the A.U.[a]	8
Chain[b]/No. of residues/missing residues	A/265/1–2, 8–9, 120–127, 166–168, 244–247 B/271/1–2, 121–126, 164–167, 246 C/269/1–3, 120–128, 166–167, 245 D/267/1–2, 8–9, 120–127, 166–167, 245–247 E/271/1–2, 121–126, 164–168 F/269/1–2, 120–126, 165–167, 220, 245–246 G/269/1–2, 120–127, 164–168 H/270/1–2, 120–128, 166–167, 245
No. of protein atoms	17,092
No. of water molecules	821
No. of reflections work/test[c]	123,288/13,575 (6,746/794)
Crystallographic *R* factor/R_{free}	0.209/0.247 (0.240/0.291)
rmsd bond lengths (Å)	0.006
rmsd bond angles/dihedrals (°)	1.3/27.7
Mean temperature factor (Å^2)	
Main chain	36.0
Side chain	36.6
Solvent	37.3

[a] Asymmetric unit.
[b] The eight molecules were identified with the chain indicators A–H.
[c] The numbers in parentheses are for the highest resolution shell (2.13–2.00 Å).

Model Building and Crystallographic Refinement—Manual model building and corrections were carried out using TURBO-FRODO (26). Structure refinement was performed using CNS (27) including anisotropic B factor and bulk solvent correction as well as the cross-validation method (28). The R_{free} value was calculated from a random set of reflections (10%) that were omitted from structure refinement. Strict noncrystallographic symmetry was included during the first steps of the refinement. These constraints were finally released when 90% of the residues, corresponding to 89% of all atoms, were built. Solvent molecules were added as neutral oxygen atoms in the last stages of refinement when they appeared as positive peaks above 3.0–4.0 σ and displayed acceptable hydrogen bonding geometry. The final *R* and R_{free} values were 0.209 and 0.247, respectively (Table II), and the average temperature factor for all protein atoms was 36.3 Å^2. The mean coordinate error was estimated to be less than 0.28 Å (29). All of the

[1] The abbreviations used are: MES, 4-morpholineethanesulfonic acid; PMN, polymorphonuclear cell; ATR, attenuated total reflectance; FTIR, Fourier-transformed infrared; rmsd, root mean square deviation.

residues belong to the allowed regions of a Ramachandran plot, and 87.1% of them have the most favored backbone angles, as defined by PROCHECK (30).

Construction of Modified Proteins—Mutations of LukS-PV at position Thr-28 (Cys, Asp, Phe, His, Leu, Asn, and Ser) were achieved using dedicated oligonucleotides and a mutagenesis procedure similar to that of QuikChange™ mutagenesis (Stratagene), except that *Pfu* Turbo™ DNA polymerase was replaced by Arrow Taq™ DNA polymerase and T4 gp32 protein (Q-Biogene). DNA sequences corresponding to secreted proteins were previously cloned to express a glutathione *S*-transferase fusion protein into the expression vector pGEX-6P-1 (Amersham Biosciences) (31). *Escherichia coli* XL1 Blue cells (*recA1 endA1 gyrA96 thi1 hsdR17 supE44 relA1 lac* (F′ *proAB lacI*^{q} ZΔM15 *Tn*10 (*tet*^{r})) (Stratagene) were used as recipients of recombinant plasmids containing mutated proteins. *E. coli* BL21 [F$^-$, *ompT*, *hsdS* (*rB*$^-$, *mB*$^-$), *gal*] was used for overexpression of the pGEX-6P-1 glutathione *S*-transferase-fused leucotoxins as previously published (31). The proteins were purified by affinity chromatography on glutathione-Sepharose 4B followed by cation exchange fast protein liquid chromatography after the removing of the glutathione *S*-transferase tag with PreScission™ Protease (Amersham Biosciences) as previously described (32). LukS-PV G10C and LukF-PV S27C, two functional cysteine mutated proteins, were labeled with fluorescein 5-maleimide (Molecular Probes) (31, 32).

Human Polymorphonuclear Cells (PMNs) and Flow Cytometry Measurements—Human PMNs from healthy donors were purified and used to evaluate the respective binding and activity of modified proteins (4, 31) with a FACSort™ flow cytometer (Becton Dickinson) equipped with an argon laser tuned at 488 nm (33). Fluo-3 fluorescence (Molecular Probes) for Ca^{2+} entry and ethidium fluorescence were acquired with Lysis II™ software (Becton Dickinson) as previously described (22, 31). The results from at least four different donors were averaged and expressed as percentages of a control of human PMNs treated with wild type Panton-Valentine leucocidin. Base level values were obtained for each series of data from a control without toxin and were systematically subtracted from the other assays. It has been shown that LukS-PV has a high affinity for its membrane target with a dissociation constant of 0.07 nM (4), and wild type and mutated LukS-PV proteins were added at 1 nM. LukF-PV, whose dissociation constant for the PMN membrane-bound LukS-PV is 2.5 nM (2), was applied at 40 nM.

Competition experiments were performed in the absence of extracellular Ca^{2+} on PMNs previously incubated at room temperature for 10 min with 1 nM of LukS-PV. Fluorescein-labeled LukS-PV G10C or LukF-PV S27C, both at a concentration of 20 nM, and increasing concentrations of mutated LukS-PV proteins or LukF-PV (from 1 to 1000 nM), respectively, were added 15 min before reading the fluorescence. IC_{50}, the concentration of nonfluorescent competitor needed for 50% fluorescence inhibition, was determined from the best fit of independent triplicates of the residual cell fluorescence. $k_{I\,app}$, the apparent inhibition constant, was calculated as earlier reported (4, 31).

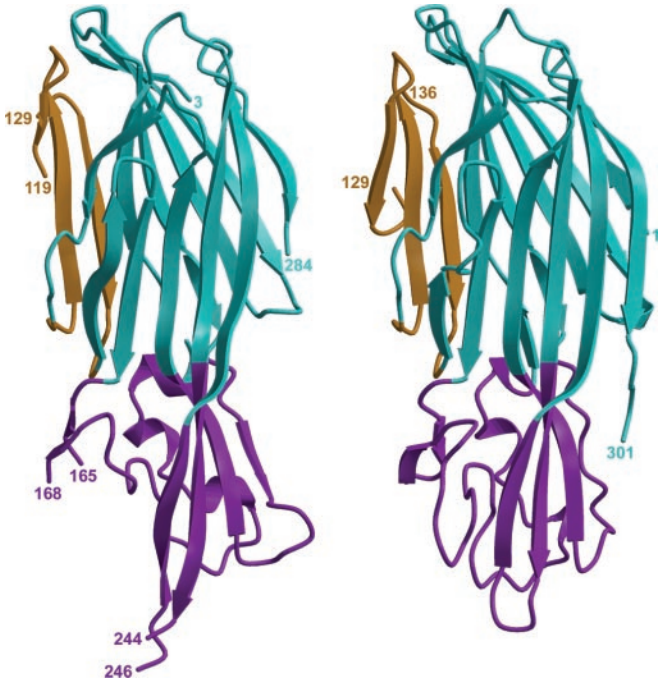

FIG. 1. **Three-dimensional structures of the two components of Panton-Valentine leucocidin.** Ribbon representation of LukS-PV (*left*) and LukF-PV (*right*). The β-sandwich, rim, and stem domains are shown in *cyan*, *magenta*, and *orange*, respectively. The N and C termini and the chain breaks are labeled.

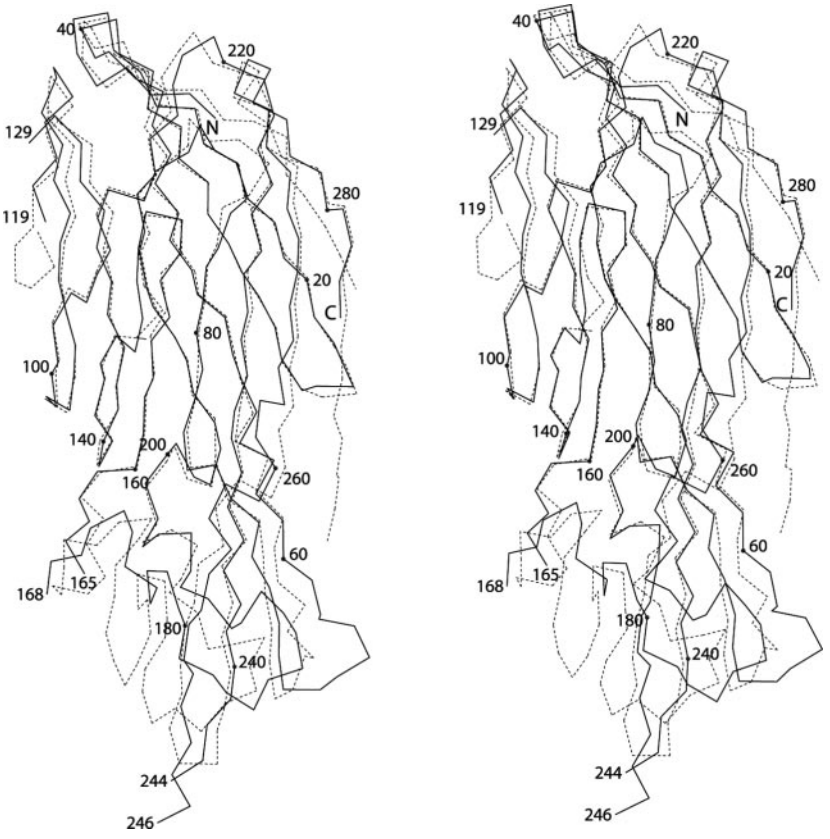

FIG. 2. **Structure superimposition of the two components of Panton-Valentine leucocidin.** Stereo view of the α-carbon trace of LukS-PV (*solid lines*) superimposed on that of LukF-PV (*dotted lines*). The zones used for the superposition comprise residues 3–59, 68–85, 87–118, 130–147, 149–165, 175–180, 192–241, 252–259, and 263–284 of LukS-PV and residues 8–64, 72–89, 92–123, 137–154, 157–173, 190–195, 207–256, 262–269, and 272–293 of LukF-PV. Every 20th Cα of LukS-PV is indicated by a *black dot* and labeled.

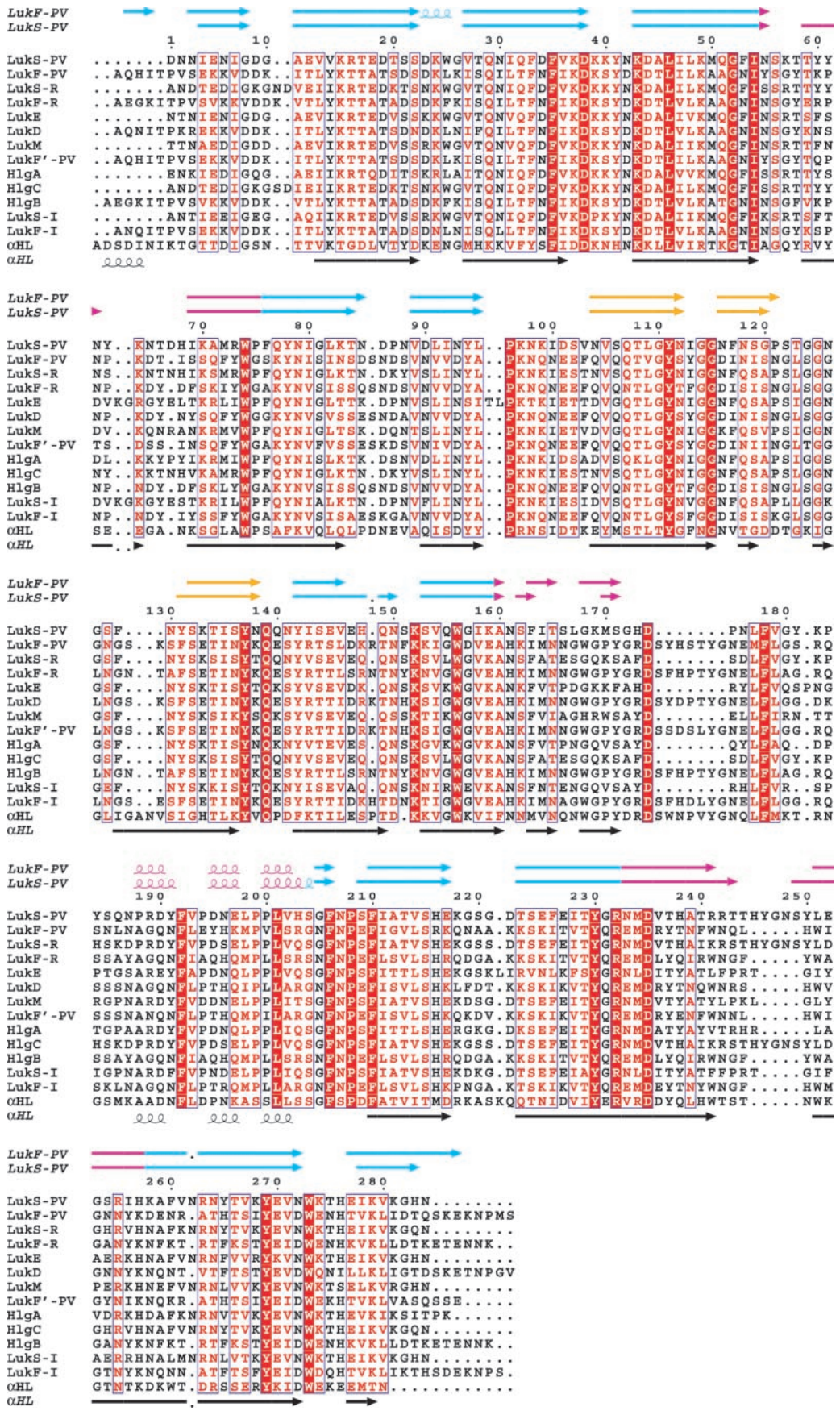

FIG. 3. **Structure-based sequence alignment for *Staphylococcus aureus* F and S proteins of bicomponent leucotoxins and α-hemolysin.** S and F proteins of each leucotoxin were grouped. The sequence numbering is for LukS-PV. Sequence homologies are highlighted in *red*, whereas sequence identities are shown as *white letters* on a *red background*. Secondary structure elements (*arrows* for β-strands and coils for α-helices) of the S and F proteins of Panton-Valentine leucocidin (colored as in Fig. 1) are indicated at the *top*, and those of α-hemolysin (*black*) are at the *bottom*.

Attenuated Total Reflectance ATR Fourier-transformed Infrared FTIR Spectroscopy—ATR-FTIR spectra were recorded as described before (34) on a Bio-Rad FTS 185 FTIR spectrometer equipped with a mercury-cadmium-tellurium detector, a KBr beamsplitter, and an attenuated total reflection attachment. Before analysis, leucotoxin samples at 0.6 mg/ml were desalted on G50 medium with 10 mM HEPES-NaOH, pH 7.0. For each experiment, 50 μg of the given desalted leucotoxin were deposited and dried in a thin layer on one side of a 10-reflection germanium crystal. The crystal was housed in a liquid cell, and spectra were collected after flushing with N_2 saturated with D_2O for ~30 min. They were analyzed with the Bio-Rad WIN-IR software package to obtain secondary structure content (34, 35). Differential spectra were obtained by subtracting the averaged spectrum of wild type LukS-PV (four samples) from the average spectrum of each LukS-PV mutant (two to four samples). To compensate for small differences in protein concentration, before subtraction, each spectrum was normalized by dividing by a scalar corresponding to the area of its amide I′ band. To express the structural changes introduced by the mutations in the polypeptide backbone, we used the COBSI (change of backbone structure and interaction) index (36). This index relates the absorbance change to the total protein absorbance integrated over the amide I′ region between 1700 and 1610 cm^{-1}. For example, a COBSI index of 1% implies that in a protein having 300 amino acid residues, like the leucotoxins components, three of these residues have changed their conformation.

Production of the Figures—Figs. 1, 2, and 7 were produced using BobScript (37). Fig. 1 was rendered using RASTER3D (38). Fig. 3 was produced using ESPript (39) with a sequence alignment edited manually using SEAVIEW (40), and secondary structure assignment was performed with STRIDE (41). Fig. 4 was produced using PyMol (DeLano, W.L. The PyMOL Molecular Graphics System (2002) DeLano Scientific, San Carlos, CA).

RESULTS

Structure Determination—Several class S proteins from different leucotoxins were expressed, purified, and subjected to crystallization. Among them, only the S component of the Panton-Valentine leucocidin (LukS-PV) gave crystals. Monoclinic and tetragonal crystals were obtained (23). The latter, which diffracts x-rays to 2.0 Å resolution, was used to solve the structure using the molecular replacement method and the previously determined three-dimensional coordinates of LukF-PV (14) as a search model. Eight molecules of LukS-PV were found in the asymmetric unit, and the refined model comprises 265–271 of 284 amino acids found in the wild type protein representing a total of 2151 residues. The 121 missing residues had poorly defined electron density and belong to the N termini of the protein and to three loops exposed to solvent (Table II). The side chains of 116 residues with also either poor or no electron density were truncated to the Cβ atom. A total of 821 water molecules were positioned in the electron density. Pairwise superimposition of the α-carbons of the eight molecules in the asymmetric unit gives root mean square deviations (rmsd) ranging from 0.09 to 0.55 Å for 259 matched atoms. Descriptions of the structure will refer to the central molecule (chain H).

Structure of LukS-PV and Comparison with Other Known Structures—The three-dimensional structure of LukS-PV was analyzed using the program PROMOTIF (42). The fold is composed of 19 strands (63.7% of residues) that form an ellipsoid and participate to four antiparallel β-sheets and three short segments of either 3_{10} (2.6%) or α (1.5%) helices. As could be anticipated from previous studies (10, 14, 43), this fold is strongly similar to that found in the crystal structures of α-hemolysin, LukF-PV, and HlgB (the F component of Panton-Valentine leucocidin and γ-hemolysin, respectively) and is arranged into the typical β-sandwich, rim, and folded stem domains (Fig. 1). The regions with the highest temperature factors, which include residues that flank the missing segments, are located at the two poles of the ellipsoid in connecting loops of the β-sandwich and rim domains and in the folded stem domain.

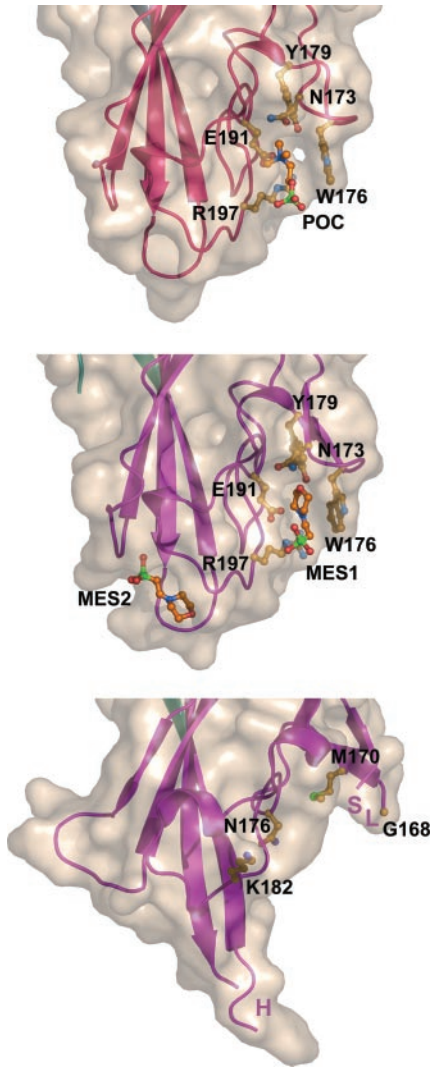

FIG. 4. **Structural variation in the rim domain of leucotoxins and lipid binding capability.** Ribbon and semi-transparent surface representation comparing the rim domains of HlgB (*top panel*), LukF-PV (*middle panel*), and LukS-PV (*bottom panel*). The phosphocholine headgroup of DiC_3PC (*POC*) and MES molecules as well as residues defining the corresponding binding sites in HlgB and LukF-PV, respectively, are shown and labeled. Carbon, nitrogen, oxygen, and phosphorous (or sulfur) atoms are *orange*, *blue*, *red*, and *green*, respectively. The binding of POC (MES) is mainly mediated by hydrophobic/van der Waals' contacts and involves a single polar interaction between the main chain nitrogen atom of residue Arg-197 and an oxygen atom of the phosphate (sulfonate) group.

Superimposition of the LukS- and LukF-PV (Protein Data Bank code 1PVL) structures using all atoms of those invariant residues previously identified (14) to play an important role for domains folding and stabilization (*i.e.* according to LukS-PV numbering: Ile-54, Tyr-78, Tyr-94, Pro-96, Tyr-142, Trp-156, Leu-201, Phe-206, Pro-208, Phe-210, and Phe-230 of the β-sandwich domain; Trp-74, Leu-177, Phe-178, Phe-192, and Asp-235 of the rim domain; and Asp-38, Tyr-111, Gly-114, Gly-115, Tyr-137, and Gln-139 of the stem domain) gives an rmsd of 1.0 Å for 207 main chain and side chain atoms. Superimposition of the LukS- and LukF-PV structures was also achieved globally and led to an rmsd value of 1.0 Å for 228 corresponding Cα atoms (Fig. 2). In comparison, superimposition of LukF-PV and HlgB (Protein Data Bank code 1LKF), whose sequences contain ~300 residues, gives an rmsd value of 1.0 Å for 292 matched Cα atoms. In fact, the structures of LukS- and LukF-PV fit much better in their β-sandwich and

TABLE III
Binding and structural variation of wild type LukS-PV and its mutants

Protein	S binding[a]	F binding[b]	COBSI index[c]	Shift β^2	Shift r
	nM	*nM*	*%*	cm^{-1}	cm^{-1}
LukS-PV wt[d]	0.04 ± 0.01	3.03	0.0	0.0	0.0
LukS-PV T28C	wt	7.31	0.54	0.7	1.4
LukS-PV T28S	wt	5.86	0.83	−0.5	0.2
LukS-PV T28H	wt	13.83	0.67	0.2	1.4
LukS-PV T28F	wt	>500	0.89	−2.3	0.4
LukS-PV T28L	4.38 ± 0.52	87	1.73	−2.5	−0.1
LukS-PV T28N	wt	>500	2.40	−3.2	1.2
LukS-PV T28D	0.13 ± 0.01	>500	1.55	−4.2	−0.4

[a] $k_{I\ app[S]}$, apparent dissociation constant of LukS-PV and its mutants for PMN cells, determined from competition experiments, using fluorescein-labeled LukS-PV G10C.
[b] $k_{I\ app[F]}$, apparent dissociation constant of LukF-PV for LukS-PV (and its mutants) bound onto PMN cells, determined using fluorescein-labeled LukF-PV S27C.
[c] The COBSI index is an estimation, obtained from differential spectra, of the conformational changes induced by the mutations (see "Experimental Procedures"). The last two columns report the shift in the position of the maximum of the two β^2 bands (cumulated) and of the random coil band, r.
[d] wt, wild type.

stem domains, with nearly all Cα atoms being matched, than in the rim domain where only 58% of Cα atoms are matched (Fig. 2). Pronounced deviations occur in four peptide segments corresponding to residues 60–67, 168–174, 181–191, and 242–251 of the rim domain. Residues 60–62 form a β-strand that is absent in the structure of LukF-PV, and residues 63–67 connect this strand to the adjacent strand of the rim β-sheet. Residues 168–171 form one short strand of the peripheral two-stranded β-sheet, and their positions are affected by the shortening of the following loop (residues 172–175) because of the deletion of seven residues in the LukS-PV sequence. Residues 181–191 form an Ω loop that is flipped with respect to that formed by residues 196–206 of LukF-PV. Finally, residues 242–251 participate to a connecting loop between the two remaining strands of the 4-stranded rim β-sheet. This loop is longer because of an insertion of five residues compared with LukF-PV. It should be noted that the changes described above are not due to crystallization artifact. Indeed, the rmsd values after pairwise superposition of the 81 α-carbons from the rim domain of the eight molecules in the asymmetric unit do not exceed 0.30 Å. These changes are neither related to the rigid body movement described after the comparison of the α-hemolysin protomer and LukF-PV or HlgB structures (13, 14). This rigid body displacement has an influence on the relative orientations of the rim and β-sandwich domains in the water-soluble monomeric forms and the α-hemolysin protomer but does not prevent fitting of individual domains.

The superimposition of the F and S structures allowed to refine sequence alignments previously performed based on either the structure of α-hemolysin alone (10, 44) or its comparison with that of LukF-PV (14) (Fig. 3). Salient features of the new structure-based sequence alignment are the following: (i) both the N and C termini of the different S sequences match exactly and they are systematically shorter than their counterparts in the F sequences; (ii) there are two insertions and two deletions of a single residue and the stem of the S proteins is shorter by two residues than that of the F proteins; (iii) as described above, there is a large deletion (six residues) in all S sequences, whereas the insertion of 5 residues is observed in half of them; and (iv) hypervariability is clustered at the N and C termini in the β-sandwich domain and spread all over the rim domain. These features may have a deep impact with respect to the function (see below).

Conformation of the Folded Stem Domain—The conformation of the stem domain of LukS-PV and its interface with the β-sandwich domain are similar to their counterparts in LukF-PV (14) (Fig. 2). Because of poorly defined electron density, six to nine residues of the stem domains found in the eight molecules of the asymmetric unit could not be traced. The missing residues belong to the C terminus of the second strand and, as in the structures of LukF-PV and HlgB, to the right-handed cross-over connection between the second and third

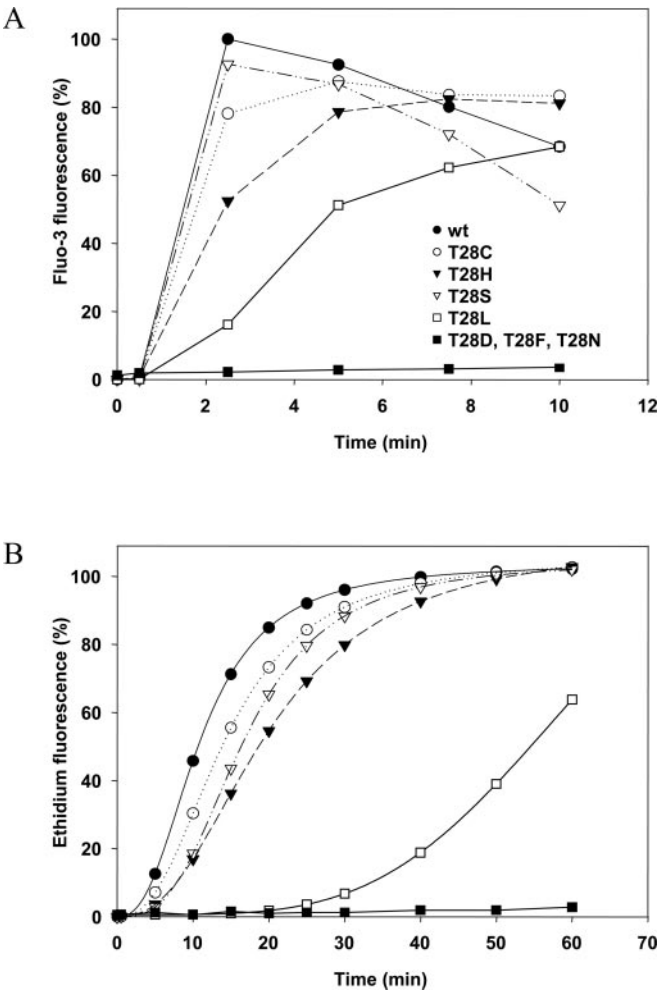

FIG. 5. **Activation and permeabilization of human PMNs by wild type LukS-PV and its mutants.** *A*, evaluation by flow cytometry of the kinetics of Ca^{2+} influx on PMNs previously loaded with 5 μM of Fluo-3 in the presence of 1.1 mM extracellular Ca^{2+}. *B*, time course of ethidium entry on PMNs previously incubated with 4 μM ethidium in the absence of extracellular Ca^{2+}. LukS-PV (wt, ●) and its mutants (1 nM) T28C (○), T28H (▼), T28S (▽), T28L (□), T28D (■), T28F (■), and T28N (■) were combined with 40 nM LukF-PV.

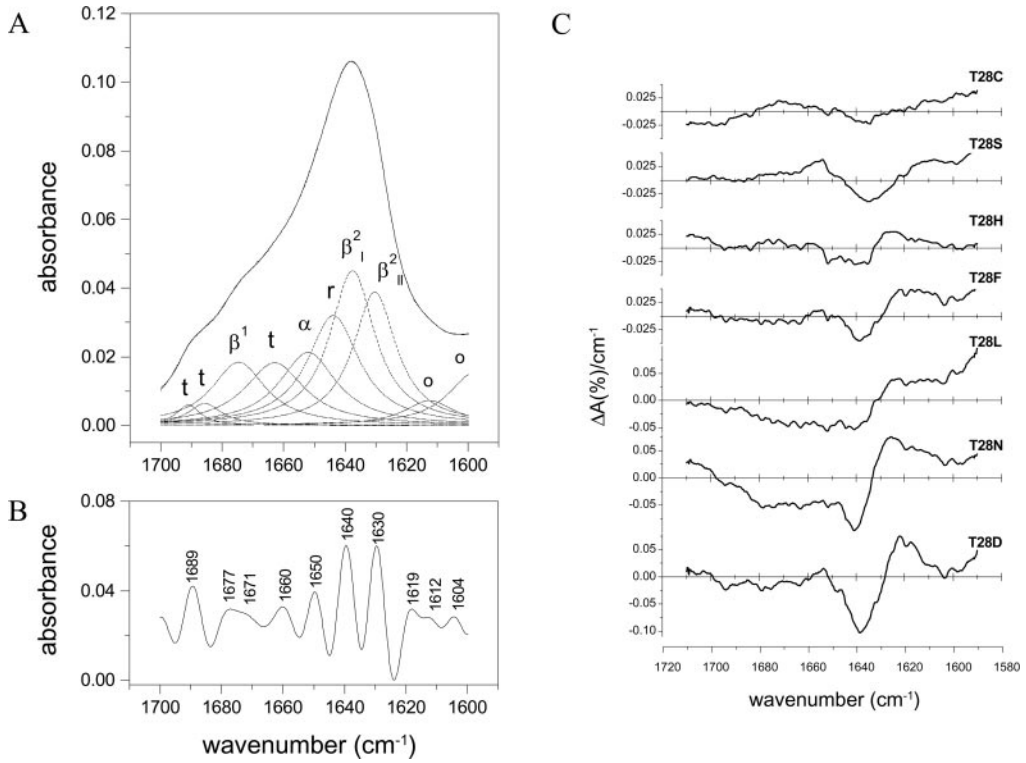

FIG. 6. **Infrared ATR data in the amide I′ region of wild type LukS-PV and its mutants.** *A*, spectrum of wild type LukS-PV (*solid lines*). *B*, spectrum deconvoluted with a resolution enhancement factor 1.6 and Bessel smoothing, which shows the presence and position of 10 components. 10 Lorentzian components with these initial positions were least squares fitted to the original data (*dotted lines* in *A*). These bands were assigned (according to Ref. 35) to: β-turn (*t*), antiparallel β-sheet (β^1), helix (α), random coil (*r*), parallel plus antiparallel β-sheet (β^2), and side chains (*o*). The resulting fit is superimposed as a *thick dotted line* to the original spectrum, from which it is almost indistinguishable. The relative area of the fitted bands was used to calculate the percentage of secondary structures, giving for wild type LukS-PV: total β, 54%; *t*, 17%; *r*, 17%; and α, 12%. *C*, differential spectra obtained by subtracting the averaged spectrum of wild type LukS-PV from the average spectrum of each LukS-PV mutant, corrected for differences in protein concentration (see "Experimental Procedures") and expressed as percentages of the amide I′ area.

strands of the folded stem β-sheet. The amino acid sequence of the cross-over connection is the less conserved part of the stem domain and, as mentioned above, it is shorter by two residues in the S proteins. However, this does not seem to induce conformational constraints that could prevent flexibility. Furthermore, SDS-PAGE of dissolved crystals revealed a single protein band that excludes any cleavage in this region.

Interactions of the Leucotoxin Components with the Membrane—The proximal position of the base of the rim domain with respect to the membrane-spanning region of the stem in the α-hemolysin heptamer and the presence in this area of numerous solvent-exposed aromatic groups provide simple geometric and chemical evidences for direct interactions of the rim domain with the lipid head groups of membranes (12). Such interactions were directly observed in difference electron density map from α-hemolysin crystals soaked in diheptanoyl phosphatidyl-choline (12) and in the crystal structure of HlgB cocrystallized with dipropanoyl phosphatidyl-choline (13). Similar interactions have also been observed in the structure of LukF-PV with a MES molecule provided by the medium used for the crystallization of the protein (3). In all cases, binding of phosphocholine or the molecular mimic occurs in a well defined cleft lined by five residues (Asn-173, Trp-176, Tyr-179, Glu-191, and Arg-197 with respect to LukF-PV numbering) that are highly conserved among α-hemolysin and F proteins of the bi-component leucotoxins (Fig. 4). These residues are borne by the polypeptide stretch that encompasses the peripheral two-stranded β-sheet and the two long consecutive loops (residues 171–208 in LukF-PV) and covers the internal face of the rim β-sheet.

As described above, this stretch of residues has a completely different conformation in the structure of LukS-PV, resulting in a different molecular surface with respect to α-hemolysin and F components (Fig. 4). In LukS-PV, the surface of the rim domain is flattened and thus appears as less globular, leading to the opening of the lipid head-binding cleft, which rather forms a valley. These features and the sequence variability observed in S *versus* F components result in a different chemical environment in this area, where Trp-176 of LukF-PV is replaced by Gly-168, Tyr-179 by Met-170 and Glu-191 is replaced by Asn-176. In addition, Arg-197 of LukF-PV and Lys-182 of LukS-PV, which occupy equivalent position in the sequence alignment, have their Cα atoms separated by 9 Å and their side chains pointing in opposite direction. Thus, the binding of phospholipid as observed in α-hemolysin and F components is precluded in LukS-PV. Accordingly, LukS-PV, which was also crystallized in the presence of MES buffer (23) does not display any of the two MES-binding sites observed in the structure of LukF-PV (Fig. 4). The secondary MES-binding site found in the rim domain of LukF-PV forms a shallow depression involving the side chains of three other strictly conserved residues among α-hemolysin and F proteins (Trp-256, Trp-261, and Asn-200). In this context, it is noteworthy that there is no accessible tryptophan residue in the rim domain of LukS-PV and that other aromatic residues are distributed differently. For instance, three accessible tyrosine residues are found at the very tip of the rim domain in the LukS-PV molecule.

Functional and Biophysical Properties of LukS-PV Mutants—Mutagenesis at position Thr-28 of LukS-PV (Cys, Asp, Phe, His, Leu, Asn, and Ser) was first evaluated in terms of binding to PMNs (Table III). The $k_{I\ app}$ for wild type LukS-PV was 0.04 nM. Only one mutant, T28L, showed a lowered affinity

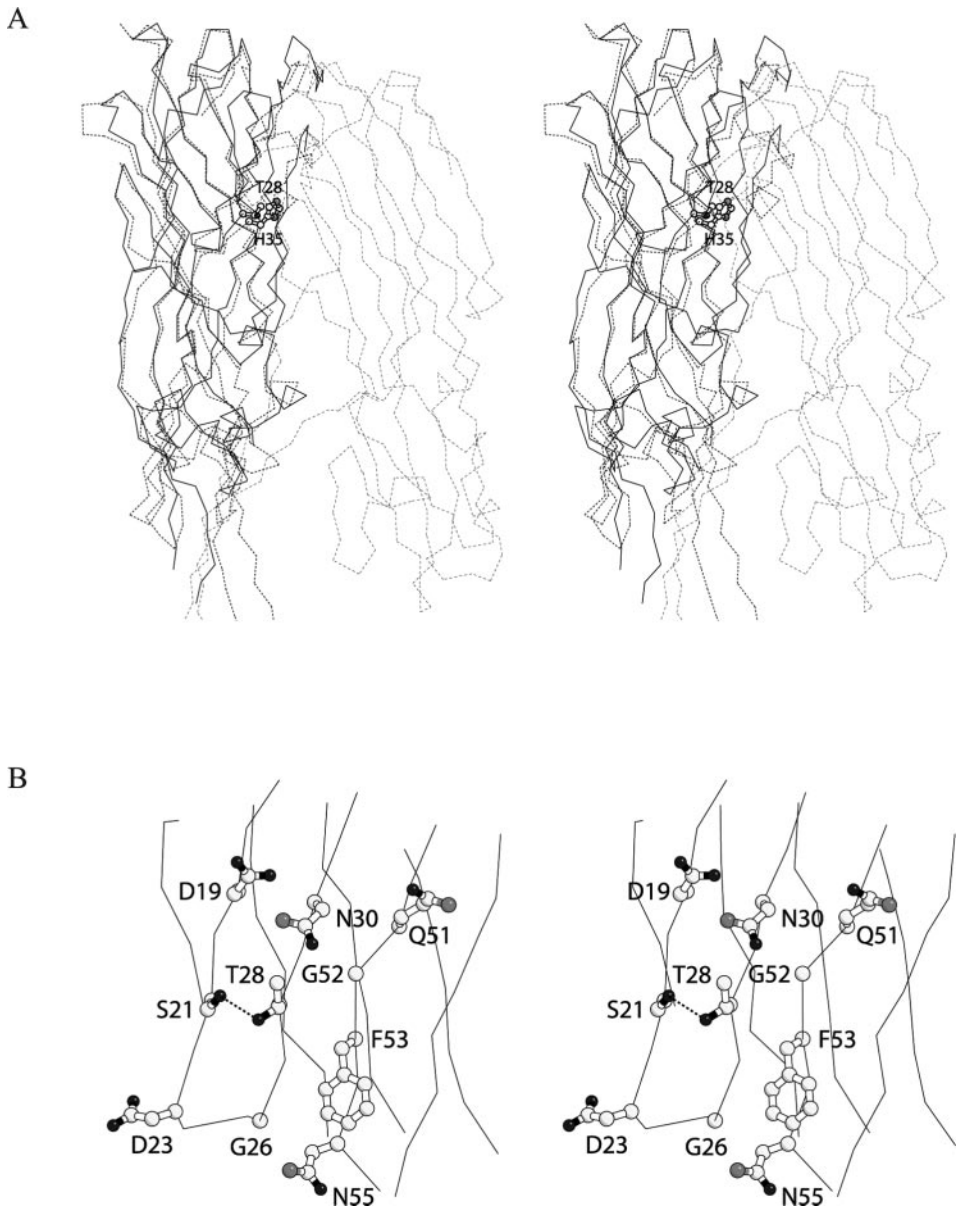

FIG. 7. **Comparison of LukS-PV and α-hemolysin and the environment around Thr-28.** *A*, stereo view of the α-carbon trace of LukS-PV (*solid lines*) superimposed on one protomer from the α-hemolysin heptamer (*dotted lines*). The superposition was based on the β-sandwich domains (rmsd = 0.9 Å for 111 Cα atoms). The side chains of Thr-28 and His-35 of LukS-PV and α-hemolysin, respectively, are represented as ball-and-stick and labeled. A second protomer (±1 neighbor) of α-hemolysin is also shown to illustrate the protomer-protomer interface. For sake of clarity, the view is centered on the core of the proteins, and the stem of α-hemolysin thus appears truncated at the bottom of the figure. *B*, close-up view of the chemical environment around Thr-28. The *dotted lines* indicate the hydrogen bond formed between the OG1 atom of Thr-28 and the OG atom of Ser-21. Carbon, nitrogen, and oxygen atoms are *white*, *gray*, and *black*, respectively.

($k_{I\,app}$ = 4.38 nM) for which there is no straight explanation. The binding of fluorescein-labeled LukF-PV S27C to each of the LukS-PV protein previously bound to the membrane was next evaluated. According to this property, LukS-PV mutants could be divided into three categories: (i) mutants that did not allow any specific binding of LukF-PV, *i.e.* T28D, T28F, and T28N with a $k_{I\,app}$ of >500 nM; (ii) LukS-PV T28L that was largely affected ($k_{I\,app}$ = 87 nM); and (iii) mutants that authorized almost normal LukF binding properties, *i.e.* T28S, T28C, and T28H (Table III). The Ca^{2+} entry activity of couples composed of a given LukS-PV mutant and wild type LukF-PV showed a good correlation with the binding of LukF-PV to that mutant (Fig. 5*A*). For instance, LukS-PV T28S and T28C induced a Ca^{2+} entry almost comparable with that of the wild type Panton-Valentine leucocidin, and LukS-PV T28H showed a slight decrease that became markedly significant with the substitution to leucine. Finally, LukS-PV T28D, T28F, and T28N did not generate any calcium entry activity. The occurrence of functional pores permeable to the monovalent ethidium cation varies in a similar and even more pronounced manner. Again, LukS-PV T28H was found a lesser inducer than T28S and T28C, whereas T28L showed very low activity, and T28D, T28F, and T28N were all inactive (Fig. 5*B*).

The effect of these mutations on the secondary structures of LukS-PV were analyzed by ATR-FTIR. The spectra of wild type LukS-PV and mutant proteins were all clearly similar, with the amide I′ band always peaked in the region 1634–1640 cm^{-1} to indicate a prevalent β structure mainly composed of antiparallel strands (Fig. 6*A*). A detailed analysis of the relative amounts of the different secondary structure elements composing the proteins was obtained by a deconvolution procedure followed by a curve fit to the original spectra (Fig. 6, *A* and *B*). The results are consistent with the x-ray structure described herein, within the experimental resolution of the FTIR tech-

nique (typically from 5 to 10%). Differential spectra evidenced slight changes introduced by the mutations (Fig. 6*C*). Minimal differences were seen with T28C, T28S and T28H, medium changes with T28F and T28L, and the largest deviations were obtained with T28N and T28D (Fig. 6*C* and Table III). A decrease in the absorbance at 1640 cm^{-1} and an increase at 1620 cm^{-1} were generally observed, which could suggest a decrease in random coil and an increase in β structures, respectively (35). However, the curve fit procedure indicated that the observed differences, rather than being caused by a variation in the amount of secondary structures, derived from a shift of the two β^2 bands toward lower wave numbers. It might indicate a progressive strengthening of the strand to strand hydrogen bonding interactions that could derive from subtle rearrangements in the molecules, rather than representing true changes in secondary structures. In the case of T28N, the effect is boosted by a simultaneous shift of the random coil band to higher wave number (Table III).

DISCUSSION

Limited data exist on the mechanism of assembly and molecular architecture of staphylococcal leucotoxins, but their similarity in structure and in function with the single polypeptide α-hemolysin suggests that they share the same mechanism of pore formation (3, 13, 45). The three-dimensional structure of LukS-PV brings further important details about the subtle variability that can be introduced within the fold of the pore-forming leucotoxins superfamily, as defined in the SCOP (structural classification of proteins) data base (46). For instance, the different conformation observed for the rim domain of LukS-PV compared with the known structures of F monomers and of the α-hemolysin protomer illustrates the dynamic properties and molecular plasticity of these molecules. Such a conformation of the rim could only be confined to class S proteins and α-hemolysin because this domain might be locked in most class F proteins because of their longer C termini (Figs. 2 and 3). At least in the case of the Panton-Valentine leucocidin, this might be related to the propensity of LukS-PV to specifically interact with membrane compounds (4).

Whatever the multiplicity and the stoichiometry of the leucotoxin hetero-oligomer(s) formed, this involves the obligatory interaction of the S and F polypeptides (2). With that respect, it is worth mentioning that the simplest scheme in which S and F proteins alternate in the final assembly, as recently evidenced by single molecule fluorescence microscopy (17), requires only two types of subunit-subunit interface (S-F and F-S), whereas all other arrangements in a random assortment generate two additional interfaces (S-S and F-F). In the structure of the α-hemolysin heptamer (12) (Protein Data Bank code 7AHL), each protomer interacts with its ± 1 neighbors and to a much less extent with its ± 2 neighbors, burying approximately one-third of the solvent-accessible surface area. Interacting residues are spread over one face of the protomer core, principally in the β-sandwich domain, and in the amino latch, the stem β strands, and the triangle region, which connects the stem domain to the protomer core. Except for those residues belonging to the amino latch and to the stem β strands, which undergo a conformational change upon oligomerization and pore formation, the positions of the backbone atoms of residues involved in interprotomer interactions in the α-hemolysin heptamer structure are globally well conserved in the structure of the soluble forms of LukF- and LukS-PV (Fig. 7*A*). However, and as pointed out in an earlier analysis (10), residues whose side chains are in interaction at the protomer-protomer interface of the α-hemolysin heptamer are poorly conserved among leucotoxins F and S proteins. One such residue, His-35 plays a critical role in the assembly and function of α-hemolysin. This residue has been the focus of several substitutions, most of them reducing heptamer formation and the hemolytic activity (47–51). His-35 is located on the second strand of the β-sandwich domain (Fig. 7*A*) and is systematically replaced by a threonine and a serine in S and F proteins, respectively, with the exception of LukD (Fig. 3). The effect of the substitutions on the corresponding residue of LukS-PV, *i.e.* Thr-28, points also out the importance of this position for the assembly and function of leucotoxins, in accordance with a previous study performed on HlgA and HlgC (33). Indeed, our functional results indicate that the T28L, T28F, T28N, and T28D mutants are inactive, whereas T28H and T28C have only decreased activity and T28S remains fully active. Thr-28 is exposed on one side of LukS-PV and together with residues Asp-23, Ser-21, Gly-26, Phe-53, and Asn-55 defines a crevice that provides an opening for ready access (Fig. 7*B*). Thus, mutations at this position are well tolerated in terms of the tertiary structure of the monomer because the new side chains may project toward this crevice. In contrast, these mutations are much less easily accommodated in terms of activity because the steric and/or electrostatic repulsion they might introduce could prevent the correct oligomerization. Accordingly, substitutions of Thr-28 with serine and cysteine residues that were similar in size and polarity clearly preserved both structure and activity.

In the absence of any structural information for an assembled oligomer, our data illustrate the important functional role played by sequence and tertiary structure microheterogeneities for both molecular recognition to specific membrane partners and the assembly of the bipartite leucotoxins. They may pave the way for future prospective studies aiming at the determination of essential residues for protein-protein interactions.

Acknowledgments—We are grateful to the skillful technical assistance of D. Keller for the purification of LukS-PV. We thank the scientific staff of the European Synchrotron Radiation Facility (Grenoble, France) for excellent data collection facilities.

REFERENCES

1. Prévost, G., Menestrina, G., Colin, D. A., Werner, S., Bronner, S., Serra, M. D., Baba Moussa, L., Coraiola, M., Gravet, A., and Monteil, H. (2003) in *Pore-Forming Peptides And Protein Toxins* (Menestrina, G., Serra, M. D., and Lazarovici, P., eds) pp. 3–26, Taylor and Francis Publishers, London
2. Colin, D. A., Mazurier, I., Sire, S., and Finck-Barbançon, V. (1994) *Infect. Immun.* **62,** 3184–3188
3. Prévost, G., Mourey, L., Colin, D. A., and Menestrina, G. (2001) *Curr. Top. Microbiol. Immunol.* **257,** 53–83
4. Gauduchon, V., Werner, S., Prévost, G., Monteil, H., and Colin, D. A. (2001) *Infect. Immun.* **69,** 2390–2395
5. Staali, L., Monteil, H., and Colin, D. A. (1998) *J. Membr. Biol.* **162,** 209–216
6. Hensler, T., König, B., Prévost, G., Piémont, Y., Köller, M., and König, W. (1994) *Infect. Immun.* **62,** 2529–2535
7. König, B., Köller, M., Prévost, G., Piémont, Y., Alouf, J. E., Schreiner, A., and König, W. (1994) *Infect. Immun.* **62,** 4831–4837
8. König, B., Prévost, G., Piémont, Y., and König, W. (1995) *J. Infect. Dis.* **171,** 607–613
9. Colin, D. A., and Monteil, H. (2003) *Infect. Immun.* **71,** 3724–3729
10. Gouaux, E., Hobaugh, M., and Song, L. (1997) *Protein Sci.* **6,** 2631–2635
11. Menestrina, G., Serra, M. D., and Prévost, G. (2001) *Toxicon* **39,** 1661–1672
12. Song, L., Hobaugh, M. R., Shustak, C., Cheley, S., Bayley, H., and Gouaux, J. E. (1996) *Science* **274,** 1859–1866
13. Olson, R., Nariya, H., Yokota, K., Kamio, Y., and Gouaux, E. (1999) *Nat. Struct. Biol.* **6,** 134–140
14. Pédelacq, J. D., Maveyraud, L., Prévost, G., Baba-Moussa, L., Gonzalez, A., Courcelle, E., Shepard, W., Monteil, H., Samama, J. P., and Mourey, L. (1999) *Structure* **7,** 277–287
15. Sugawara, N., Tomita, T., and Kamio, Y. (1997) *FEBS Lett.* **410,** 333–337
16. Ferreras, M., Hoper, F., Dalla Serra, M., Colin, D. A., Prévost, G., and Menestrina, G. (1998) *Biochim. Biophys. Acta* **1414,** 108–126
17. Nguyen, V. T., Kamio, Y., and Higuchi, H. (2003) *EMBO J.* **22,** 4968–4979
18. Sugawara-Tomita, N., Tomita, T., and Kamio, Y. (2002) *J. Bacteriol.* **184,** 4747–4756
19. Miles, G., Movileanu, L., and Bayley, H. (2002) *Protein Sci.* **11,** 894–902
20. Gravet, A., Colin, D. A., Keller, D., Girardot, R., Monteil, H., Prévost, G., and Giradot, R. (1998) *FEBS Lett.* **436,** 202–208
21. Prévost, G., Bouakham, T., Piémont, Y., and Monteil, H. (1995) *FEBS Lett.* **376,** 135–140
22. Comai, M., Dalla Serra, M., Coraiola, M., Werner, S., Colin, D. A., Monteil, H., Prévost, G., and Menestrina, G. (2002) *Mol. Microbiol.* **44,** 1251–1267
23. Guillet, V., Keller, D., Prévost, G., and Mourey, L. (2004) *Acta Crystallogr. Sect. D Biol. Crystallogr.* **60,** 310–313

24. Vagin, A., and Teplyakov, A. (1997) *J. Appl. Crystallogr.* **30,** 1022–1025
25. Collaborative Computational Project Number 4. (1994) *Acta Crystallogr. Sect. D Biol. Crystallogr.* **50**, 760–763
26. Roussel, A., and Cambillau, C. (1989) *Silicon Graphics Geometry Partner Directory*, pp. 71–78, Silicon Graphics, Mountain View, CA
27. Brunger, A. T., Adams, P. D., Clore, G. M., DeLano, W. L., Gros, P., Grosse-Kunstleve, R. W., Jiang, J. S., Kuszewski, J., Nilges, M., Pannu, N. S., Read, R. J., Rice, L. M., Simonson, T., and Warren, G. L. (1998) *Acta Crystallogr. Sect. D Biol. Crystallogr.* **54,** 905–921
28. Brunger, A. T. (1992) *Nature* **355,** 472–475
29. Luzzati, V. (1952) *Acta Crystallogr.* **5,** 802–810
30. Laskowski, R. A., MacArthur, M. W., Moss, D. S., and Thornton, J. M. (1993) *J. Appl. Crystallogr.* **26,** 283–291
31. Baba Moussa, L., Werner, S., Colin, D. A., Mourey, L., Pédelacq, J. D., Samama, J. P., Sanni, A., Monteil, H., and Prévost, G. (1999) *FEBS Lett.* **461,** 280–286
32. Werner, S., Colin, D. A., Coraiola, M., Menestrina, G., Monteil, H., and Prévost, G. (2002) *Infect. Immun.* **70,** 1310–1318
33. Meunier, O., Ferreras, M., Supersac, G., Hoeper, F., Baba-Moussa, L., Monteil, H., Colin, D. A., Menestrina, G., and Prévost, G. (1997) *Biochim. Biophys. Acta* **1326,** 275–286
34. Menestrina, G., Cabiaux, V., and Tejuca, M. (1999) *Biochem. Biophys. Res. Commun.* **254,** 174–180
35. Byler, D. M., and Susi, H. (1986) *Biopolymers* **25,** 469–487
36. Barth, A., von Germar, F., Kreutz, W., and Mantele, W. (1996) *J. Biol. Chem.* **271,** 30637–30646
37. Esnouf, R. M. (1997) *J. Mol. Graph.* **15,** 133–138
38. Merritt, E. A., and Murphy, M. E. P. (1994) *Acta Crystallogr. Sect. D Biol. Crystallogr.* **50,** 869–873
39. Gouet, P., Courcelle, E., Stuart, D., and Metoz, F. (1998) *Bioinformatics* **15,** 305–308
40. Galtier, N., Gouy, M., and Gautier, C. (1996) *Comput. Appl. Biosci.* **12,** 543–548
41. Frishman, D., and Argos, P. (1995) *Proteins* **23,** 566–579
42. Hutchinson, E. G., and Thornton, J. M. (1996) *Protein Sci.* **5,** 212–220
43. Pédelacq, J. D., Prévost, G., Monteil, H., Mourey, L., and Samama, J. P. (2000) *Int. J. Med. Microbiol.* **290,** 395–401
44. Gouaux, E. (1998) *J. Struct. Biol.* **121,** 110–122
45. Montoya, M., and Gouaux, E. (2003) *Biochim. Biophys. Acta* **1609,** 19–27
46. Murzin, A. G., Brenner, S. E., Hubbard, T., and Chothia, C. (1995) *J. Mol. Biol.* **247,** 536–540
47. Jursch, R., Hildebrand, A., Hobom, G., Tranum-Jensen, J., Ward, R., Kehoe, M., and Bhakdi, S. (1994) *Infect. Immun.* **62,** 2249–2256
48. Krishnasastry, M., Walker, B., Braha, O., and Bayley, H. (1994) *FEBS Lett.* **356,** 66–71
49. Menzies, B. E., and Kernodle, D. S. (1994) *Infect. Immun.* **62,** 1843–1847
50. Walker, B., and Bayley, H. (1995) *J. Biol. Chem.* **270,** 23065–23071
51. Walker, B., and Bayley, H. (1995) *Protein Eng.* **8,** 491–495